THE PHOTOGRAMMETRIC RECORD

The Photogrammetric Record (2013)
DOI: 10.1111/phor.12038

GENERATION AND VALIDATION OF HIGH-RESOLUTION DEMS FROM WORLDVIEW-2 STEREO DATA

Umut G. Sefercik (ugsefercik@hotmail.com)
Bulent Ecevit University, Zonguldak, Turkey

Mehmet Alkan (alkan@yildiz.edu.tr)
Yildiz Technical University, Istanbul, Turkey

Gurcan Buyuksalih (gbuyuksalih@yahoo.com)
IMP-Bimtas, Istanbul, Turkey

Karsten Jacobsen (jacobsen@ipi.uni-hannover.de)
Leibniz Universität Hannover, Hanover, Germany

Abstract

WorldView-2 (WV-2), whose panchromatic images have a 0·5 m ground sampling distance (GSD), was launched by DigitalGlobe in 2009. It is the first commercial satellite to offer 8-band multispectral imagery with 1·8 m resolution. Due to the off-nadir sensor rotation of WV-2, it is feasible to obtain stereo coverage. Digital elevation models (DEMs) have been created with three WV-2 stereopairs of northern Istanbul with different land types and one of these is comprehensively analysed in this study. A reference DEM, developed from large-scale aerial photogrammetric mapping, together with a lidar DEM and an overlapping neighbouring WV-2 DEM, are used for validation. The generated WV-2 DEM reached, after filtering and in open areas, a standard deviation in height of approximately 1·0 GSD. A higher number of discrepancies larger than 4 m exist than would be expected from a normal distribution, influencing the standard deviation more than the normalised median absolute deviation (NMAD).

Keywords: DEM generation, high resolution, optical stereoscopy, quality evaluation, validation, WorldView-2

Introduction

Digital elevation models (DEMs) are one of the remote sensing products most in demand and are used increasingly for several applications, such as the creation of three-dimensional views and relief maps (Fraser, 2003), orthophoto generation, disaster monitoring and disaster management (Vassilopoulou et al., 2002; Navalgund et al., 2007), the establishment of geographical information systems (GIS) (Font et al., 2010), agriculture (Thompson et al.,

2001; Schmidt and Persson, 2003), forestry (Büyüksalíh et al., 2005; Stereńczak and Kozak, 2011) and drainage (Jain and Singh, 2005). Before the development of spaceborne imaging technologies, land surveying techniques and photogrammetry were the only approaches that were available for DEM generation. These techniques yield high accuracy but are time consuming. In addition, in some countries the use of aerial images is restricted. Today, optical satellite images compete with aerial images for mapping applications.

The elevation models must conform to predetermined quality standards and user requirements. The quality of the model includes two main components: accuracy and morphologic detail. Accurate elevation information is crucial for mapping products if satellite data are to be used (Li, 1998). Based on optical space images, the accuracy of the generated DEMs is mainly dependent upon the ground resolution, base-to-height ratio, image contrast and terrain roughness (Jacobsen, 2003). IKONOS, QuickBird, OrbView, WorldView-1 (WV-1), GeoEye-1 and WorldView-2 (WV-2) as well as Pleiades were launched sequentially and are capable of providing a ground resolution of up to 0·5m.

The automated DEM generation from WV-2 stereopairs in Istanbul, Turkey, is described and analysed. The next section presents the characteristics of the study area and the applied WV-2 dataset. This is followed by an explanation of the methodology used for DEM generation, including scene orientation and matching, digital surface model (DSM) generation, DSM to DEM conversion by filtering, and gap filling. Next, the DEM evaluation process and results are presented, followed by the conclusions from this research.

Study Area and WorldView-2 Dataset

The study area is located north-west of Istanbul, Turkey; it is adjacent to the Black Sea coast with the Bosporus at the eastern limit of the site (Fig. 1). The terrain is flat to undulating, with a few steeper parts (Fig. 2); it includes forests, water bodies, partially worked quarries and gravel pits. The height of the terrain ranges from -43 m, due to opencast mining, to 165 m. Fig. 1 shows an overlay of the three WV-2 pan-sharpened scenes used in this study and Table I indicates the stereo combinations. The satellite has the advantage of fast rotation, which allowed the imaging of the three stereomodels (six images) from the same orbit within 92 s. The physical ground sampling distance (GSD) for the nadir view of WV-2 is 0·46 m. Due to the incidence angles used in stereomodel 1, the GSD reaches up to 0·57m (Table I); nevertheless, the images are resampled by DigitalGlobe to 0·5m GSD. Mainly the left-hand (most westerly) stereomodel has been analysed due to the available reference data and the satisfactory overlap with the centre stereomodel.

DEM Generation Methodology

As already noted, spaceborne remote sensing has become an alternative method to aerial photography and other methods for DEM generation (Jacobsen, 2002; Toutin and Cheng, 2002; Fraser, 2003; Amato et al., 2004; Büyüksalíh et al., 2004; Reinartz et al., 2010; Poli and Toutin, 2012). This is possible with optical and radar stereoscopy (radargrammetry) or interferometric synthetic aperture radar (InSAR). Stereopairs may be taken from the same orbit by using forward and backward images (along-track) or taken from two adjacent orbits (cross-track) (Jacobsen, 2003; Krishna et al., 2008). With the fast rotational capability of WV-2, along-track stereopairs can be achieved, and illumination

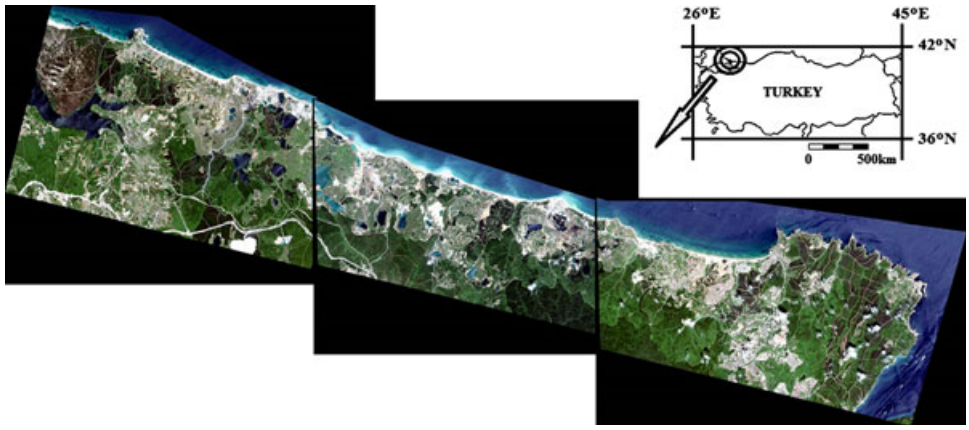

FIG 1. Pan-sharpened WV-2 stereo scenes of the study area (left to right: stereomodels 1, 2 and 3).

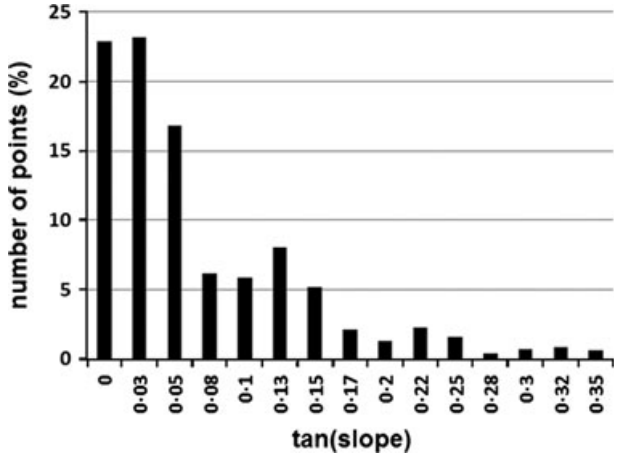

FIG 2. Frequency distribution of the terrain inclination in the study area.

changes in images taken on different days can be avoided. The required scene orientations were made by a bias-corrected rational polynomial solution using the program RAPORI, developed by Leibniz University, Hanover, Germany, that utilises approximately equally distributed ground control points (GCPs), selected from aerial images. The object coordinates of the GCPs were accurate; however, identification of the points in the WV-2 images with 0·5 m GSD was quite difficult, which restricted the accuracy and created errors. The direct sensor orientation, expressed by rational polynomial coefficients (RPCs), is not accurate enough for the required DEMs. As a result, the orientations have been determined by a bias-corrected RPC solution with RAPORI, which uses GCPs for the correct location (Grodecki, 2001; Jacobsen, 2007; Srivastava et al., 2008). Table II shows the root mean square (RMS) discrepancies at the finally used GCPs of each stereomodel.

Due to several misidentifications of GCPs, the adjustment of the bias-corrected RPC of the WV-2 scenes required blunder detection by data snooping. For the elimination of

TABLE I. Technical data of WV-2 stereomodels with viewing configuration.

Stereo-model number	*Base-to-height ratio*	*Maximum incidence angle (°)*	*Maximum physical GSD (m)*	*Viewing configuration*
1 (Red)	1 : 1·43	27·1	0·52 × 0·57	
2 (Blue)	1 : 1·79	24·1	0·50 × 0·55	
3 (Green)	1 : 1·73	21·5	0·49 × 0·53	

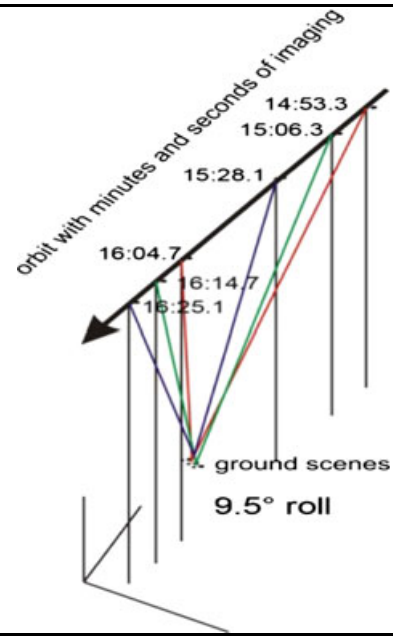

systematic effects, a bias correction with a 2D-affine transformation was necessary. A shift alone was not sufficient, and the individual affine coefficients are significant in most cases.

The image matching has been performed with grey-value images that were generated from the RGB images, based on least squares matching with region growing. Approximation seed points (corresponding points in both images of the stereopair) are required. From these seed points, the least squares matching expands to the neighbourhood until the sub-area concerned is completely filled. This method works very well in open and built-up areas without tall buildings; however, problems were identified with the method in respect of forested areas. For this reason, the images have been scaled down linearly by a factor of 10. The region growing worked very well with the scaled-down images. The corresponding image points were used as seed points for the full-resolution images. This corresponds to a pyramid method for the approximations with just two levels. For the least squares matching, only points above a correlation threshold of 0·6 in the 10×10 pixel template used were accepted.

TABLE II. RMS discrepancies in X, Y, Z coordinates at GCPs determined by bias correction.

Stereomodel	*Number of GCPs*	*RMS X (m)*	*RMS Y (m)*	*RMS Z (m)*
1	14	0·41	0·20	0·64
2	15	0·57	0·36	0·48
3	14	0·52	0·36	1·28

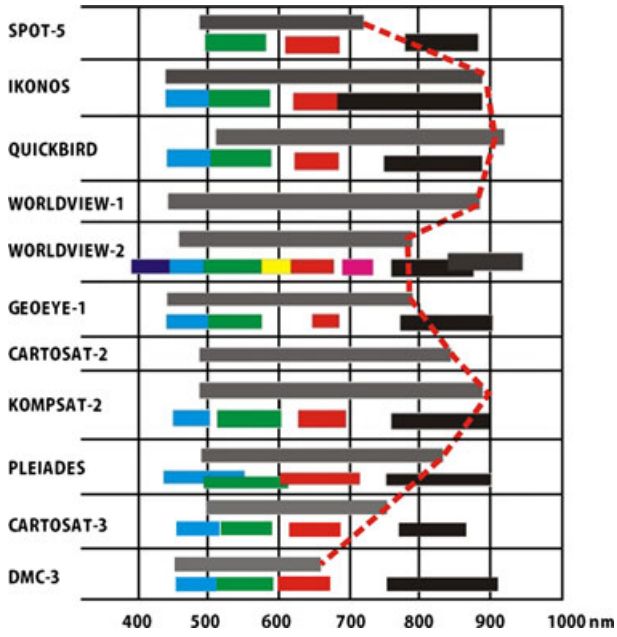

FIG 3. The spectral range of high-resolution optical satellite imagery. The high-resolution panchromatic band is shown in grey, with the longest wavelength detectable shown by the pecked line(Büyüksalíh et al., 2012).

The spectral range of the high-resolution panchromatic band for the latest high-resolution satellites WV-2 and GeoEye-1 has been compared with IKONOS, QuickBird and WV-1 equivalents (Fig. 3). The spectral range of the WV-2 panchromatic band is closer to the real panchromatic character for the visible range, thus simplifying the pan-sharpening; however, the image matching in forested areas is more challenging due to the missing good vegetation contrast evident in the near infrared (Büyüksalíh and Jacobsen, 2005). The grey-value variation in forested areas is not as poor as for SPOT-5; nevertheless, the standard deviation of the grey values in forested areas in the WV-2 images used, where the correlation coefficients are less than 0·6, is typically below ± 10 grey values. Fig. 4 shows the quality of image matching with the colour-coded correlation coefficients according to their location (a) and frequency distribution (b).

Corresponding to the frequency distribution of the correlation coefficients in Fig. 4(b), approximately 8% of the points are neglected in stereomodel 1 if a threshold of 0·6 is used. Regarding Fig. 4(a), the coefficients are close to 1·0 in built-up areas, which is compatible with the range of the road network. The coefficients are smaller for agricultural areas and are often below 0·6 in forests. The matching fails for water bodies. Towards the eastern edge (right-hand side), a strip is outside of the stereo coverage; however, the other areas with low correlations are associated with forest. In the unmatched forested areas, the RMS of the grey values is in the range of ± 2 to ± 10, which is too low for acceptable matching results. Based on the corresponding image coordinates by intersection, a DSM with a point spacing of 3 m was generated (Fig. 5) using BLUH (bundle block adjustment of Leibniz Universität Hannover) software. The intersection was quite successful with RMS parallaxes in the range of 0·2 to 0·3 m (0·4 to 0·6 pixels).

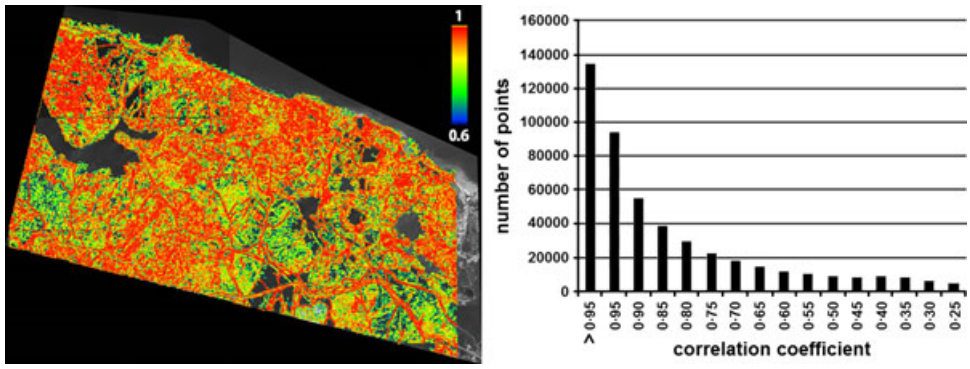

(a) (b)

FIG 4. (a) Colour-coded image of magnitude of correlation coefficients (0·6 to 1·0) depending upon the location in one image. (b) Frequency distribution of correlation coefficients.

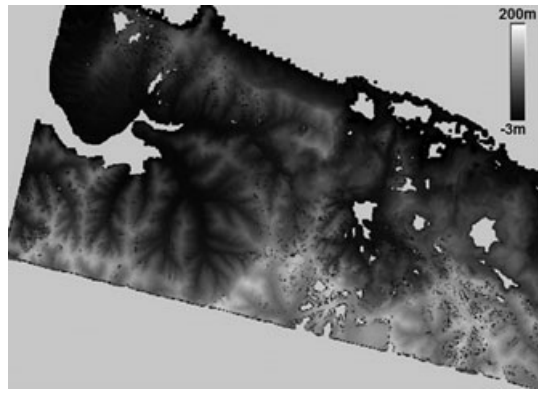

FIG 5. Grey-value coded WV-2 DSM.

DEM EVALUATION AND RESULTS

The DSM that was generated was compared with both a reference DEM based on digital aerial photographs with a 10 cm GSD and a lidar DEM. The reference and lidar DEMs were generated by the Greater Municipality of Istanbul between 2005 and 2007 and during 2012, respectively; both have a vertical accuracy of 10 cm to 1 m with a 3 m original grid spacing. The reference DEM as well as the lidar DEM include the height of bare ground areas. A direct comparison of the DSM generated by WV-2 images with the reference DEM is influenced by vegetation and building heights. By filtering the DSM, points that are not located on the ground and have ground heights in the neighbourhood can be eliminated (Day et al., 2013). This process has limitations in a forest with full canopy where no ground heights are available in the DSM. Due to this fact, the DSM has been filtered by RASCOR software to obtain a DEM which is closer to the reference DEM; 41% of the WV-2 elevation points were removed. While there appears to be a strong decrease in

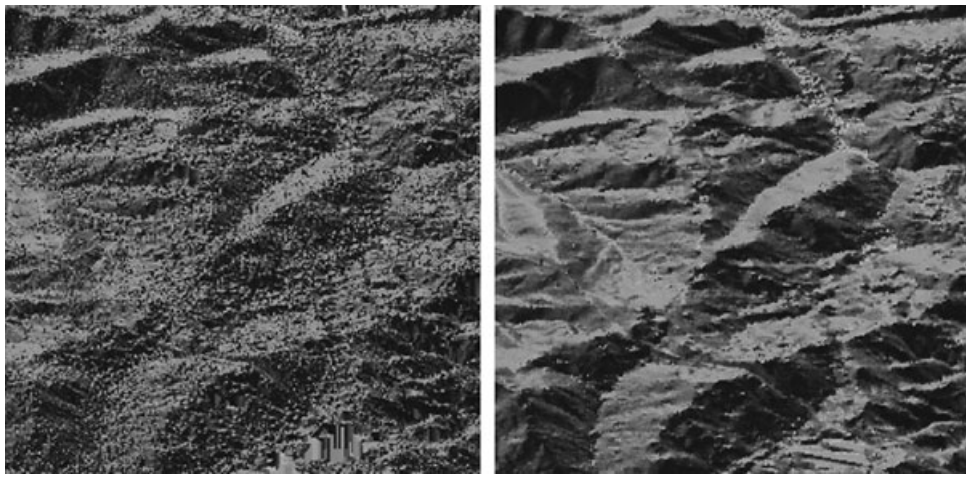

FIG 6. Influence of filtering: WV-2 DEM, before (left) and after (right) filtering.

height information, the quality of the model actually improved, as only elevated points above the ground surface were removed. Fig. 6 demonstrates the result of filtering in a difficult sub-area of stereomodel 1.

Several challenges have been encountered. Firstly, working quarries and gravel pits create problems. Airborne images for the reference DEM were taken between 2005 and 2007, the WV-2 images in 2011 and the lidar data in 2012. During this time some quarries and gravel pits have lowered their ground height by up to 32 m. Deposits in surrounding areas accumulate, which also influences the ground height. Smaller gaps of up to 10 m have been interpolated, which introduces discrepancies due to rough terrain. Originally, the reference height model was available in the Turkish national coordinate system, which was later transformed into the Universal Transverse Mercator (UTM) projection. Because of problems with imperfectly known datums, shifts of the reference models against the WV-2 DEM were determined by adjustment and respected in further analysis. Furthermore, it is necessary to analyse the DEM separately for each of the four main land classes (Fig. 7). Finally, only the data in open areas are treated as reliable because of the influence of vegetation; additionally, altered ground heights in areas covered by quarries and gravel pits should not be included in standard deviation figures.

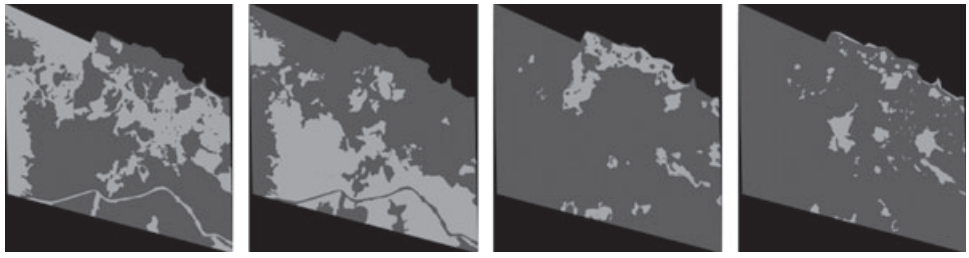

FIG 7. Layers for different land classes, shown in light grey.

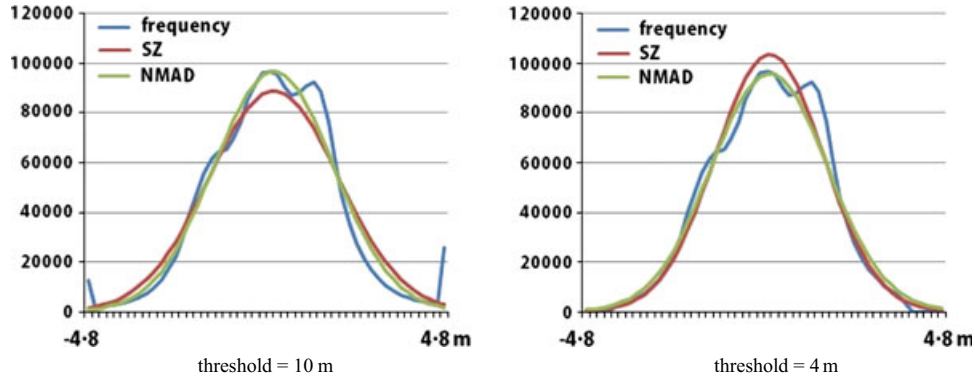

FIG 8. Frequency distributions of height discrepancies of WV-2 DEM against the reference DEM in open areas with superimposed normal distribution based on SZ and NMAD.

The accuracy figures for describing the geometric quality of a DEM are complex. Beside the standard deviation of the height (SZ or σ_Z), the normalised median absolute deviation (NMAD) is used. NMAD is the median absolute deviation (MAD) multiplied by 1·48 to reach the same probability of 68% as σ_Z. Thus, in the case of normally distributed discrepancies σ_Z and NMAD should be identical. Nevertheless, as shown in Figs. 8 to 11, the frequency distributions of height discrepancies between the DEMs usually show a higher percentage of larger discrepancies as compared with a normal distribution; this is caused by problems with the surface which, even after filtering and classification, may be influenced by residual features not belonging to the bare ground category. The threshold values of linear errors with 90 or 95% probability levels (LE90 and LE95, respectively) should not be used as accuracy figures because they do not present the entire range of discrepancies. In addition, it is debateable if a threshold for accepting height discrepancies should be used for the computation of accuracy figures and, if so, what this threshold should be. Large height discrepancies may be caused by matching blunders or by the comparison of a ground point with a point located on vegetation or buildings. Matching blunders are rare and mostly caused by poor contrast, but such points are usually eliminated in advance by the threshold for the correlation coefficient. In addition, for this analysis, points exceeding a slope to neighbouring points of 60° have not been included in the comparison. Such points may be located directly beside buildings or rocks and cause problems for the interpolation routine.

The shortest distance between points on two elevation models that are being compared is not the vertical direction but the Euclidian distance. The Euclidian standard deviations are approximately 1·0% below σ_Z; for this reason, they are not shown.

Table III shows a clear dependency of the standard deviation on the threshold for accepting large discrepancies while the dependency is smaller for NMAD. The frequency distributions (Figs. 8 to 11) demonstrate that the discrepancies exceeding 4 m do not belong to the normal distribution (σ_Z); even a threshold of 4 m is too large for the comparison with both the lidar DEM and the overlapping neighbouring WV-2 DEM. Nevertheless, a threshold of 4 m for accepting height discrepancies is an operational compromise for all the datasets used.

The next question to answer is which accuracy figure is the best value for expressing the standard deviation of the height discrepancies: is this the classical RMS formula listed

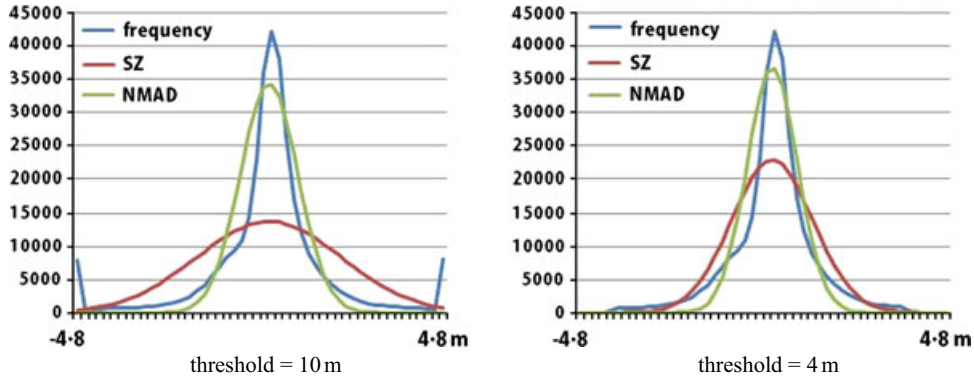

FIG 9. Frequency distributions of height discrepancies of WV-2 DEM against lidar DEM in open areas with superimposed normal distribution based on SZ (σ_Z) and NMAD.

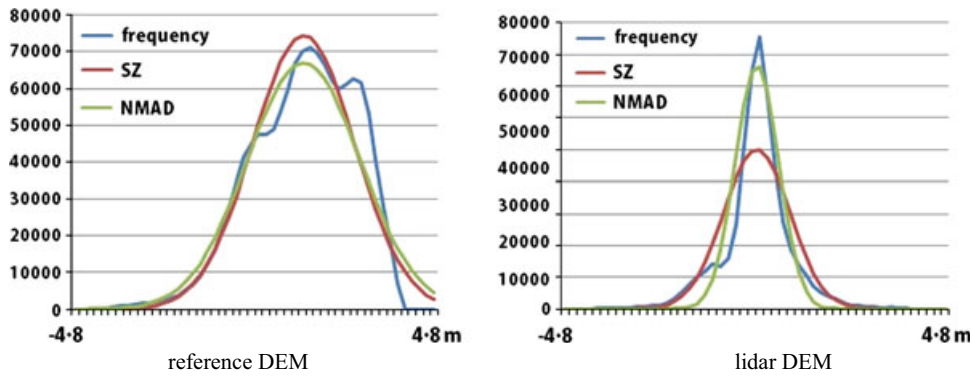

FIG 10. Frequency distributions of height discrepancies of WV-2 DEM against reference and lidar DEMs after filtering with a threshold for height differences of 4 m.

above as σ_Z (SD) or should NMAD be used? The frequency distributions in Figs. 8 to 11 demonstrate that the superimposed normal distribution based on NMAD as the standard deviation describes much better the frequency distributions, rather than the normal distribution based on SZ. A higher number of larger discrepancies influence σ_Z as it is based on the sum of the squares of differences; their influence on NMAD is only via the median. The difference between σ_Z and NMAD is smaller for filtered data as compared to the original data, confirming that the filtering eliminates several points not belonging to the bare ground classification.

The quality depends upon the slope according to a function $a + b \times \tan(slope)$. For horizontal areas the discrepancies compared with the lidar DEM, and also the independent overlapping WV-2 DEM, are in the NMAD range of slightly below 1·0 GSD. This corresponds to the system accuracy of matching which, under good conditions, leads to a standard deviation in the height of approximately 1·0 GSD.

The accuracy figures quoted are limited to open areas without trees, quarries or gravel pits. The accuracy of the heights in forests, as well as the heights in quarries and gravel

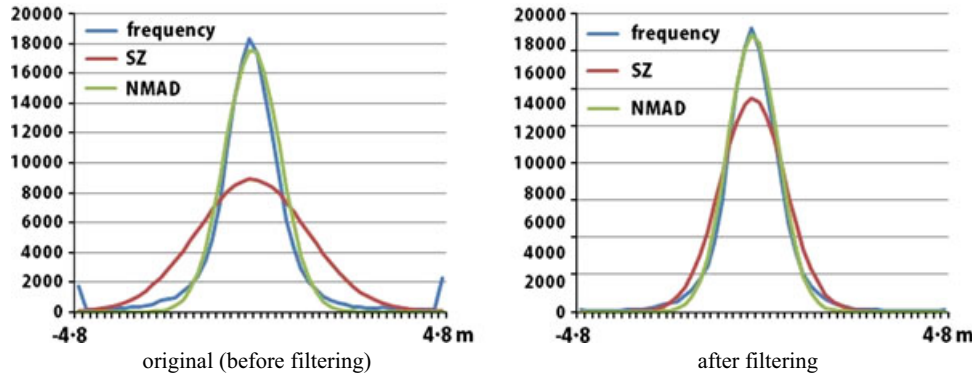

FIG 11. Frequency distributions of height discrepancies of WV-2 DEM against the overlapping WV-2 DEM before and after filtering, using a threshold for height differences of 10 m.

TABLE III. Accuracy of the WV-2 DEM (m) compared with the reference, lidar and overlapping (neighbouring) WV-2 DEMs, limited to open areas. The upper half of the table relates to the original data and the lower half to filtered data. Computations relate to accepting values below thresholds of 10 and 4 m.

Compared DEM	*% exceeding threshold*	σ_Z	*NMAD*	σ_Z *as a function of the slope*	*NMAD as a function of the slope*
			Original		
Reference	0·6% > 10 m	1·78	1·64	1·64 + 0·11 × tan(slope)	1·24 + 0·69 × tan(slope)
Reference	3·7% > 4 m	1·48	1·60	1·33 + 0·23 × tan(slope)	1·11 + 0·77 × tan(slope)
Lidar	9·6% > 10 m	1·93	0·77	0·73 + 0·80 × tan(slope)	0·55 + 1·89 × tan(slope)
Lidar	15·2% > 4 m	1·09	0·68	0·55 + 0·49 × tan(slope)	0·52 + 1·41 × tan(slope)
Neighbouring WV-2	1·7% > 10 m	1·48	0·75	1·48 + 0·00 × tan(slope)	0·75 + 0·00 × tan(slope)
Neighbouring WV-2	4·9% > 4 m	0·95	0·72	0·82 + 0·24 × tan(slope)	0·58 + 0·96 × tan(slope)
			Filtered		
Reference	0·3% > 10 m	1·57	1·61	1·34 + 0·27 × tan(slope)	1·61 + 0·00 × tan(slope)
Reference	4·0% > 4 m	1·39	1·54	1·22 + 0·19 × tan(slope)	1·54 + 0·00 × tan(slope)
Lidar	0·05% > 10 m	0·90	0·55	0·72 + 0·19 × tan(slope)	0·46 + 0·95 × tan(slope)
Lidar	2·6% > 4 m	0·85	0·55	0·68 + 0·19 × tan(slope)	0·45 + 0·95 × tan(slope)
Neighbouring WV-2	0·02% > 10 m	0·88	0·68	0·62 + 0·54 × tan(slope)	0·49 + 1·33 × tan(slope)
Neighbouring WV-2	0·4% > 4 m	0·82	0·68	0·61 + 0·47× tan(slope)	0·49 + 1·25 × tan(slope)

pits, cannot be determined by a comparison with reference DEMs. Tree heights and the height changes over time cannot be expressed by a standard deviation: this has to be described with other figures.

CONCLUSION

With a sufficient number of GCPs, the influence of the scene orientation is insignificant when compared with the influence of the object point determination in a stereomodel. For the comparison of height, model datum problems have to be solved in advance by a shift of one DEM to the other by adjustment. A comparison of a DSM with a reference DEM does not lead to usable accuracy information. Only a DEM can be compared with another DEM; the influence of vegetation, buildings or height changes in quarries and gravel pits should

not be expressed using a standard deviation. For this reason, a comparison must be limited to open areas not influenced by such distortions.

The analysed DEM, but also sometimes the reference DEM, includes some points not belonging to bare ground, requiring filtering both for achieving the final DEM and also as a precondition for an accuracy analysis. By invoking filtering, blunders are eliminated; this means expensive triple stereo scenes can be avoided if they are not required for viewing into narrow streets or in steep mountainous terrain. The accuracy figure for characterising the height quality should express the whole discrepancy population, visible as a frequency distribution. With a normal distribution based on NMAD, the frequency distributions can be expressed very well, while the classical RMS formula leads to results that are too pessimistic. For this reason, NMAD should be used as the primary accuracy figure. The dependency of the accuracy upon the terrain slope has to be acknowledged.

The height models determined by the matching of WV-2 stereo scenes are leading to very satisfactory results with a height accuracy of about 1·0 GSD for open areas. Under operational conditions, better accuracy cannot be expected. This quality is in the same range as that of the reference DEM that is based on aerial images. In Turkey, the restrictions on aerial images can be circumvented by using such high-resolution space images.

REFERENCES

Amato, R., Dardanelli, G., Emmolo, D., Franco, V., Lo Brutto, M., Midulla, P., Orlando, P. and Villa, B., 2004. Digital orthophotos at a scale of 1:5000 from high resolution satellite images. *International Archives of Photogrammetry and Remote Sensing*, 35(B4): 593–598.

Büyüksalíh, G., Koçak, G., Oruç, M., Akçin, H. and Jacobsen, K., 2004. Accuracy analysis, DEM generation and validation using Russian TK-350 stereo-images. *Photogrammetric Record*, 19(107): 200–218.

Büyüksalíh, G. and Jacobsen, K., 2005. DEM generation and validation based on optical satellite systems. EARSeL Workshop on 3D-Remote Sensing, Porto, Portugal. 7 pages (on CD-ROM).

Büyüksalíh, G., Koçak, G., Topan, H., Oruç, M. and Marangoz, A., 2005. SPOT revisited: accuracy assessment, DEM generation and validation from stereo SPOT 5 HRG images. *Photogrammetric Record*, 20(110): 130–146.

Büyüksalíh, G., Baz, I., Alkan, M. and Jacobsen, K., 2012. DEM generation with WorldView-2 images. *International Archives of Photogrammetry, Remote Sensing and Spatial Information Sciences*, 39(B1): 203–207.

Day, D., Jacobsen, K., Passini, R. and Quillen, S., 2013. A study on accuracy and fidelity of terrain reconstruction after filtering DSMs produced by aerial images and airborne LiDAR surveys. ASPRS Annual Convention, Baltimore, USA. 8 pages (on CD-ROM).

Font, M., Amorese, D. and Lagarde, J.-L., 2010. DEM and GIS analysis of the stream gradient index to evaluate effects of tectonics: the Normandy intraplate area (NW France). *Geomorphology*, 119(3–4): 172–180.

Fraser, C. S., 2003. Prospects for mapping from high-resolution satellite imagery. *Asian Journal of Geoinformatics*, 4(1): 3–10.

Grodecki, J., 2001. IKONOS stereo feature extraction – RPC approach. ASPRS Annual Conference, St Louis, USA. 7 pages (on CD-ROM).

Jacobsen, K., 2002. Comparison of high resolution mapping from space. INCA Workshop, Ahmedabad, India. 16 pages (on CD-ROM).

Jacobsen, K., 2003. DEM generation from satellite data. EARSeL, Ghent, Belgium. 13 pages (on CD-ROM).

Jacobsen, K., 2007. Orientation of high resolution optical space images. ASPRS Annual Conference, Tampa, Florida, USA. 9 pages (on CD-ROM).

Jain, M. K. and Singh, V. P., 2005. DEM-based modelling of surface runoff using diffusion wave equation. *Journal of Hydrology*, 302(1–4): 107–126.

Krishna, B. G., Amitabh, Srinivasan, T. P. and Srivastava, P. K., 2008. DEM generation from high resolution multi-view data product. *International Archives of Photogrammetry, Remote Sensing and Spatial Information Sciences*, 37(B1): 1099–1102.

Li, R., 1998. Potential of high-resolution satellite imagery for national mapping products. *Photogrammetric Engineering & Remote Sensing*, 64(12): 1165–1170.

NAVALGUND, R. R., JAYARAMAN, V. and ROY, P. S., 2007. Remote sensing applications: an overview. *Current Science*, 93(12): 1747–1766.

POLI, D. and TOUTIN, T., 2012. Review of developments in geometric modelling for high resolution satellite pushbroom sensors. *Photogrammetric Record*, 27(137): 58–73.

REINARTZ, P., D'ANGELO, P., KRAUSS, T., POLI, D., JACOBSEN, K. and BUYUKSALIH, G., 2010. Benchmarking and quality analysis of DEM generated from high and very high resolution optical stereo satellite data. *International Archives of Photogrammetry, Remote Sensing and Spatial Information Sciences*, 38(1). 6 pages (on CD-ROM).

SCHMIDT, F. and PERSSON, A., 2003. Comparison of DEM data capture and topographic wetness indices. *Precision Agriculture*, 4(2): 179–192.

SRIVASTAVA, P. K., SRINIVASAN, T. P., GUPTA, A., SINGH, S., NAIN, J. S., AMITABH, S. P., PRAKASH, S., KARTIKEYAN, B. and KRISHNA, B. G., 2008. Advanced studies in strip pair processing of Cartosat-1 data. *Photogrammetric Record*, 23(123): 290–304.

STEREŃCZAK, K. and KOZAK, J., 2011. Evaluation of digital terrain models generated in forest conditions from airborne laser scanning data acquired in two seasons. *Scandinavian Journal of Forest Research*, 26(4): 374–384.

THOMPSON, J. A., BELL, J. C. and BUTLER, C. A., 2001. Digital elevation model resolution: effects on terrain attribute calculation and quantitative soil-landscape modeling. *Geoderma*, 100(1–2): 67–89.

TOUTIN, T. and CHENG, P., 2002. QuickBird – a milestone for high resolution mapping. *Earth Observation Magazine*, 11(4): 14–18.

VASSILOPOULOU, S., HURNI, L., DIETRICH, V., BALTSAVIAS, E., PATERAKI, M., LAGIOS, E. and PARCHARIDIS, I., 2002. Orthophoto generation using IKONOS imagery and high-resolution DEM: a case study on volcanic hazard monitoring of Nisyros Island (Greece). *ISPRS Journal of Photogrammetry and Remote Sensing*, 57(1–2): 24–38.

Résumé

Le satellite WorldView-2 (WV-2), dont les images panchromatiques ont un pas d'échantillonnage au sol de 0,5 m, a été lancé par DigitalGlobe en 2009. Il s'agit du premier satellite commercial offrant 8 bandes spectrales et 1,8 m de résolution. Grâce à sa capacité de rotation par rapport au nadir, il est possible d'obtenir une couverture stéréoscopique. Des modèles numériques d'élévation (MNE) ont été créés à partir de trois couples stéréoscopiques d'images WV-2 au nord d'Istanbul sur différents types de terrain, et l'un d'entre eux est étudié dans cet article de manière approfondie. Un MNE de référence, réalisé par photogrammétrie aérienne dans le cadre d'une cartographie à grande échelle avec une maille de 3 m, a été utilisé pour la validation. Il apparaît que le MNE WV-2 est plus exact que les autres MNE dans des zones dégagées, et la qualité des détails morphologiques est supérieure.

Zusammenfassung

WorldView-2 (WV-2) ist seit 2009 aktiv, hat eine Boden-Pixelgröße von 0·5 m und ist der erste kommerzielle Satellit mit 8-Band Multispektralbildern mit 1·8 m Auflösung. WV-2 bietet die Möglichkeit einer flexiblen Stereoerfassung. Eines der Digitalen Höhenmodelle (DEM), die aus drei WV-2 Stereopaaren über dem nördlichen Istanbul mit verschiedenen Landschaftstypen abgeleitet wurden, wird intensiv in dieser Studie analysiert. Als Referenz liegen Höhenmodelle aus großmaßstäblicher Luftbildaufnahme und LiDAR vor, außerdem wurden überlappende WV-2 Modelle miteinander verglichen. Mit dem erzeugten WV-2 Höhenmodell wurden nach Filterung in den offenen Gebieten Standardabweichungen der Höhen von etwa einem Bodenpixel erreicht. Mit einer Toleranzgrenze von 4 m treten mehr große Abweichungen auf als es einer Normalverteilung entspricht. Dieses beeinflusst die Standardabweichung stärker als die Normalised Median Absolute Deviation (NMAD). Mit einer Normalverteilung basierend auf NMAD werden die Häufigkeitsverteilungen der Höhen sehr gut modelliert, aus diesem Grund sollte NMAD für die Genauigkeitsspezifikation von Höhenmodellen verwendet werden.

Resumen

WorldView-2 (WV-2), cuyas imágenes tienen un tamaño de píxel de 0·5 m, se lanzó por DigitalGlobe en 2009. Es el primer satélite comercial en ofrecer imágenes multiespectrales de 8 bandas con una resolución de 1·8 m. Gracias a la vista aponadiral del sensor es posible obtener pares estereoscópicos. A partir de tres pares estereoscópicos WV-2 se han generado modelos de elevación (DEM) del norte de Estambúl con diferentes tipos de territorio. Un de ellos se analiza en este estudio. Para la validación se usa de referencia un DEM derivado de cartografía de gran escala fotogramétrica con un espaciado de 3 m. El DEM derivado de WV-2 ha probado ser más preciso que los otros DEMs en áreas abiertas y tener mayores detalles morfológicos.